Weld Pool Convection and Its Effect

Demonstrated for the first time are 3-D convection in moving arc weld pools and its effect on penetration, segregation and porosity

BY S. KOU AND Y. H. WANG

ABSTRACT. A mathematical model has been developed for the first time to account for convection and temperature distributions in moving weld pools driven by buoyancy, electromagnetic and surface tension forces. The assumption of infinitely thick workpieces and the "a priori" specification of the weld pool shape, which were used in some previous models developed for stationary weld pools, are not necessary, thus making the present model much more useful—particularly where the matter of full or partial penetration in workpieces of finite thickness is concerned.

Very good agreement was obtained between computed and experimentally observed fusion boundaries, thus verifying the validity of the model. The arc efficiency and the spatial distributions of the electric current and heat flux used in the computations were based on experimentally measured results, in order to insure that the verification was appropriate.

The convection patterns and weld penetrations due to individual driving forces were demonstrated separately, in order to show the distinct differences among themselves and at the same time help explain those due to the combined driving forces—particularly the double circulation loops in the weld pool.

The computed results are in good agreement with reported experimental observations. They agree with the important findings of Heiple, *et al.*, on the role of surface tension gradient in weld pool convection and weld penetration. Macrosegregation of solute in the weld was discussed in light of the computed results on weld pool convection, and the computed results agree with the reports of Houldcroft, Savage, *et al.*, and Seretsky, *et al.*, on weld macrosegregation. Finally, based on the computed convection patterns, it was postulated that, as compared to the buoyancy force and the surface tension gradient acting in the absence of surface active agents, the electromagnetic force and the surface tension gradient acting in the presence of surface active agents tend to produce a convection pattern more favorable for removal of gas bubbles from the weld pool.

S. KOU and Y. H. WANG are, respectively, Professor and Graduate Student in the Department of Metallurgical and Mineral Engineering, University of Wisconsin, Madison, Wis.

Introduction

Weld pool convection can strongly affect the structure and properties of the resultant welds. Variations in weld characteristics which are likely to occur from changes in weld pool convection are: weld penetration, macrosegregation, gas porosity, solidification structure, undercutting and surface smoothness. Apparently, the quantitative understanding of convection and heat flow in weld pools is of considerable practical interest. Mathematical models describing convection and heat flow in weld pools are essential, not only because of the quantitative understanding they provide, but also because of the difficulties associated with the experimental measurements of weld pool convection. These difficulties are mainly due to the fact that only surface flow, rather than the overall convection pattern in the weld pool, can be observed. In fact, due to arc glow, even the observation of surface flow can be rather inconvenient.

Recently, major progress in understanding weld pool convection and its effect on weld penetration has been made by two groups of investigators. First, a series of experimental studies has been conducted by Heiple, *et al.* (Refs. 1–6), and important findings on the effect of surface active agents on weld penetration have been made. Second, a mathematical model was developed by Oreper, *et al.* (Ref. 7), to describe, for the first time, two-dimensional weld pool convection and heat flow in stationary arc weld pools driven by the buoyancy, electromagnetic and surface tension forces. Other related quantitative studies on weld pool convection and heat flow are those by Kou, *et al.* (Ref. 8), Oreper, *et al.* (Ref. 9), and Chan, *et al.* (Ref. 10).

The main purpose of this paper is to provide a quantitative tool for studying weld pool convection and weld penetration in more practical situations, *i.e.*, in moving weld pools and in workpieces of finite thickness, where weld penetration is most critical. Another purpose of this paper is to discuss macrosegregation and porosity in the weld from the viewpoint of three-dimensional weld pool convection. It should be pointed out here that the present work has been carried out in conjunction with the current research program on heat flow and solidification in GTA welding of aluminum alloys at the University of Wisconsin (Ref. 11). For this reason, weld pool convection and weld penetration in 6061 aluminum alloy have been computed in this paper. The quantitative information provided in the present work has so far proved to be very useful for our solidification work. However, the computer model, computed results and conclusion in the present study are equally applicable to other materials.

The experimental measurements on the arc efficiency and the spatial distributions of the electric current and heat flux are described elsewhere (Refs. 12, 13) and, therefore, will not be repeated here.

Formulation

Figure 1A shows a schematic sketch of an arc welding system. The heat source is moving at a constant speed, U. As a result

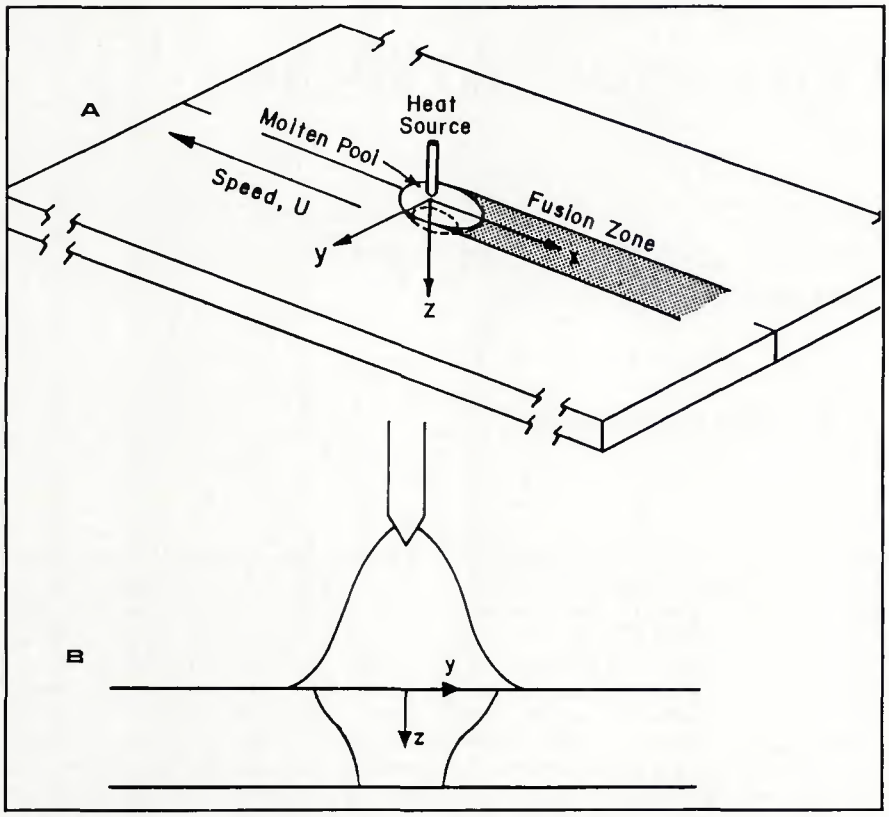

Fig. 1—Schematic sketch of (A) the arc welding system, and (B) front view of the arc and the weld pool it produces

of the heat input, a weld pool is created under the heat source. The coordinate system (x-y-z) moves with the electrode at the same speed, and its origin coincides with the center of the electrode. Figure 1B is a schematic sketch of the front view of the arc and the weld pool it produces.

The arc plasma, which acts as a distributed source of heat and electric current, impinges on the weld pool. This provides an incident flux of thermal energy and electric current at the free surface of the weld pool.

Convection in the weld pool, as pointed out previously (Refs. 7, 8), is due to three distinct forces:

1. The electromagnetic force, which is caused by the interaction between the divergent current path in the weld pool and the magnetic field it generates.
2. The buoyancy force, which is caused by the temperature gradients within the weld pool.
3. The surface tension gradient, which is caused by the temperature gradients at the free surface and possibly the surface active agents in the pool.

In the present paper, the problem is formulated as follows:

1. The convection is considered laminar, in view of the small size of the weld pool. The free surface is considered flat, which is reasonable for GTA welding with a current not much higher than 200 A (Refs. 14, 15).
2. The weld pool shape is unknown, rather than specified "a priori"; it is computed and compared with the observed fusion boundary. For this reason, the effect of weld pool convection on weld penetration can be studied.
3. The heat source is moving, rather than stationary. In other words, convection and heat flow are no longer symmetrical with respect to the center of the heat source, and the problem, therefore, becomes three-dimensional. Although the computation of convection and heat flow is considerably more complicated than in the case of stationary weld pools, the model developed in the present study is much more useful, since the vast majority of arc welding practices involve a moving heat source and weld pool.
4. The arc efficiency used in the computation is based on the measured results from calorimeters (Ref. 12). The reproducibility of the measurements was excellent, the errors being less than ±2%.
5. The spatial distributions of the electric current and heat flux on the free surface are based on measured results, using the split anode method (Ref. 13).
6. The thickness of the workpiece is finite, rather than infinite, which was the case in previous studies (Refs. 7, 8). The weld pool can be either full- or partial-penetrating, depending on the level of heat input and the nature of weld pool convection. This allows convection and heat flow to be studied in workpieces of finite thickness, where weld penetration is most critical.

Table 1—Symbols and Definitions

a	effective radius of heat flux
b	effective radius of electric current
$\vec{B}$	magnetic flux vector
C_L	specific heat of liquid
C_S	specific heat of solid
E	welding voltage
$\vec{E}$	electric field vector
$\vec{F}_b$	body force
g	workpiece thickness
$\vec{g}$	gravitational acceleration
H	enthalpy per unit mass
$\vec{H}$	magnetic field vector
ΔH	heat of fusion
I	welding current
I_r	radial component of current density vector
I_z	axial component of current density vector
$\vec{J}$	current density vector
k	thermal conductivity
k_L	thermal conductivity of liquid
k_S	thermal conductivity of solid
q	heat flux
T	temperature
T_a	ambient temperature
T_o	reference temperature
T_L	liquidus temperature
T_S	solidus temperature
U	welding speed
u	x-component of velocity vector
v	y-component of velocity vector
$\vec{V}$	velocity vector
w	z-component of velocity vector
x,y,z	coordinates
β	thermal expansion coefficient
γ	surface tension
$\partial\gamma/\partial T$	surface tension temperature coefficient
η	arc efficiency
μ	viscosity
μ_L	viscosity of liquid
μ_m	magnetic permeability
μ_S	viscosity of solid
ρ	density
τ	shear stress

The governing equations for the problem are as follows:

The equation of continuity

$$\nabla \cdot \vec{V} = 0 \qquad (1)$$

The equation of motion

$$\rho(\vec{V} \cdot \nabla)\vec{V} = -\nabla P - [\nabla \cdot \tau] + \vec{F}_b \qquad (2)$$

The equation of energy

$$\vec{V} \cdot \nabla(\rho H - P) = \nabla \cdot (k \nabla T) \qquad (3)$$

The symbols in the above equations and their definitions are given in Table 1.

The body force in the equation of

Table 2—Physical Properties Used for Calculation

β	$= 1.0 \times 10^{-4}\,°C^{-1}$	ρ	$= 2700\ kg/m^3$
μ_m	$= 1.26 \times 10^{-6}$ H/m	C_s	$= 1066$ J/kg°C
$\partial\gamma/\partial T$	$= -0.35 \times 10^{-3}\ kg/s^2{}°C$	C_L	$= 1066$ J/kg°C
T_L	$= 652°C$	k_S	$= 168$ W/m°C
T_S	$= 582°C$	k_L	$= 108$ W/m°C
T_a	$= 25°C$	μ_S	$= 1.0 \times 10^5$ kg/m s
ΔH	$= 3.95 \times 10^5$ J/kg	μ_L	$= 1.0 \times 10^{-3}$ kg/m s

motion, F_b, can be expressed as follows (Ref. 8):

$$\underset{\text{body force}}{\vec{F}_b} = \underset{\text{electromagnetic force}}{\vec{J} \times \vec{B}} - \underset{\text{buoyancy force}}{\rho\,\beta\,\vec{g}\,(T - T_o)} \tag{4}$$

As shown in Equation (4), the body force incorporated both the electromagnetic and the buoyancy forces. The remaining driving force for convection, *i.e.*, the surface tension gradient, is treated as a boundary condition, as will be shown later.

The buoyancy force is obtained from the equation of energy, *i.e.*, Equation (3). The electromagnetic force, on the other hand, may be obtained from Maxwell's equations in a way similar to that in a previous report (Ref. 8). Since the characteristic times associated with electrical conduction are on the order of 10^{-12} s, and the welding speed is very slow in comparison, the arc can be considered quasi-static.

The boundary conditions for the solution of Equations (1-4) will need to express the physical facts of symmetry with respect to the central plane of the weld (the x-z plane), and that the velocities in the solid workpiece (with respect to the moving coordinate) have the magnitude of the welding speed U and the direction in the x-direction. In addition, the following boundary conditions are used:

$$q = \frac{3\eta\,EI}{\pi a^2} \exp\left(\frac{x^2 + y^2}{-a^2/3}\right) \text{ at } z = 0 \tag{5}$$

specifying the heat flux from the arc;

$$J_r = \frac{3I}{\pi b^2} \exp\left(\frac{x^2 + y^2}{-b^2/3}\right) \text{ at } z = 0 \tag{6}$$

specifying the current flux from the arc;

$$J_z = 0 \text{ at } z = g \tag{7}$$

specifying zero current flux at bottom of workpiece. And

$$\mu \frac{\partial u}{\partial z} = -\frac{\partial T}{\partial x}\frac{\partial \gamma}{\partial T} \tag{8}$$

$$\mu \frac{\partial v}{\partial z} = -\frac{\partial T}{\partial y}\frac{\partial \gamma}{\partial T} \tag{9}$$

$$w = 0 \tag{10}$$

Equations (8-10) apply to the free surface of the weld pool, *i.e.*, at z = 0. In the case of full penetration, they also apply to the bottom free surface, *i.e.*, at z = g. Equations (8-10) express the fact that the rate at which shear is being transferred into the weld pool (LHS) is equal to the surface tension gradient (RHS), as caused by the temperature dependence of the surface tension, $\partial\gamma/\partial T$. $\partial\gamma/\partial T$ is usually negative, *i.e.*, the surface tension of the liquid metal decreases with increasing temperature. However, surface active agents, such as S and O in liquid steel, can make $\partial\gamma/\partial T$ less negative or even positive (Ref. 2). The heat loss from the top and bottom of the workpiece has been described elsewhere (Ref. 16) and, therefore, will not be repeated here.

The governing equations and the boundary conditions were cast into the finite difference form and were solved numerically. The details of the numerical method employed are described in a separate report (Ref. 17). The physical properties used for calculation are given in Table 2. A 26 × 12 × 13 unevenly spaced grid was used. The typical computer time requirements were about 21 min CPU time of Univac digital computer. In fact, the computation method was so effective that the computer program could even be run on a PDP 11-73 microcomputer in our welding laboratory.

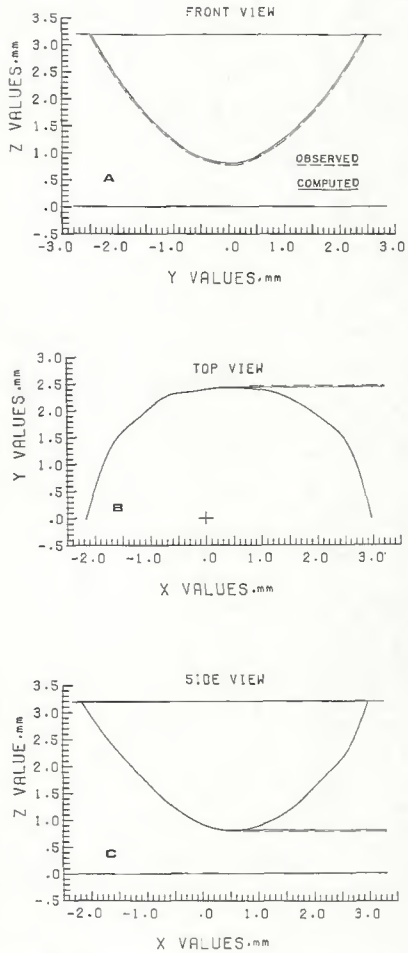

Fig. 2—Comparison between computed and observed fusion boundaries in a 3.2 mm thick 6061 aluminum plate. 100 A, 11 V and 5.5 mm/s (13 ipm): (A) front view; (B) top view; (C) side view

Computed Results

Comparison with Observed Fusion Boundary

Figure 2 shows the computed results corresponding to the first entry in Table 3. It should be pointed out again that the arc efficiency and the spatial distributions of the electric current and heat flux were based on experimentally measured results, in order to be able to properly test the validity of the computed results. As shown, the agreement between the calculated and observed fusion boundaries is very good.

Table 3—Input Parameters Used for Calculations and Calculated Depth/Width Ratios and Maximum Velocities

Run No.	Figure No.	Heat Input ηEI, W	Heat Flux Radius a, mm	Current I, A	Current Flux Radius b, mm	Surface Tension Coeff. $\partial\gamma/\partial T$, $kg/s^2{}°C$	Coefficient of Thermal Expansion β, $°C^{-1}$	Depth/ Width Ratio	Maximum Velocity mm/s
1	2	836	3.0	100	2.0	-0.35×10^{-3}	1.0×10^{-4}	0.47	–
2	3	836	3.0	100	2.0	-0.35×10^{-3}	1.0×10^{-4}	0.47	2348
3	4A	836	3.0	–	–	–	1.0×10^{-4}	0.38	9
4	4B	836	3.0	100	2.0	–	–	0.66	176
5	–	836	3.0	100	3.0	–	–	0.50	88
6	4C	836	3.0	–	–	-0.35×10^{-3}	–	0.33	3087
7	5	836	3.0	–	–	0.35×10^{-3}	–	0.66	2883
8	6	836	3.0	100	2.0	0.35×10^{-4}	1.0×10^{-4}	0.66	699

Note—Voltage: 11 V; electrode: 2.4 mm (3/32 in.) diameter and 50 deg angle; shielding gas: pure argon; welding speed: 5.5 mm/sec (13 ipm); workpiece: 6061 aluminum, 3.2 mm thick.

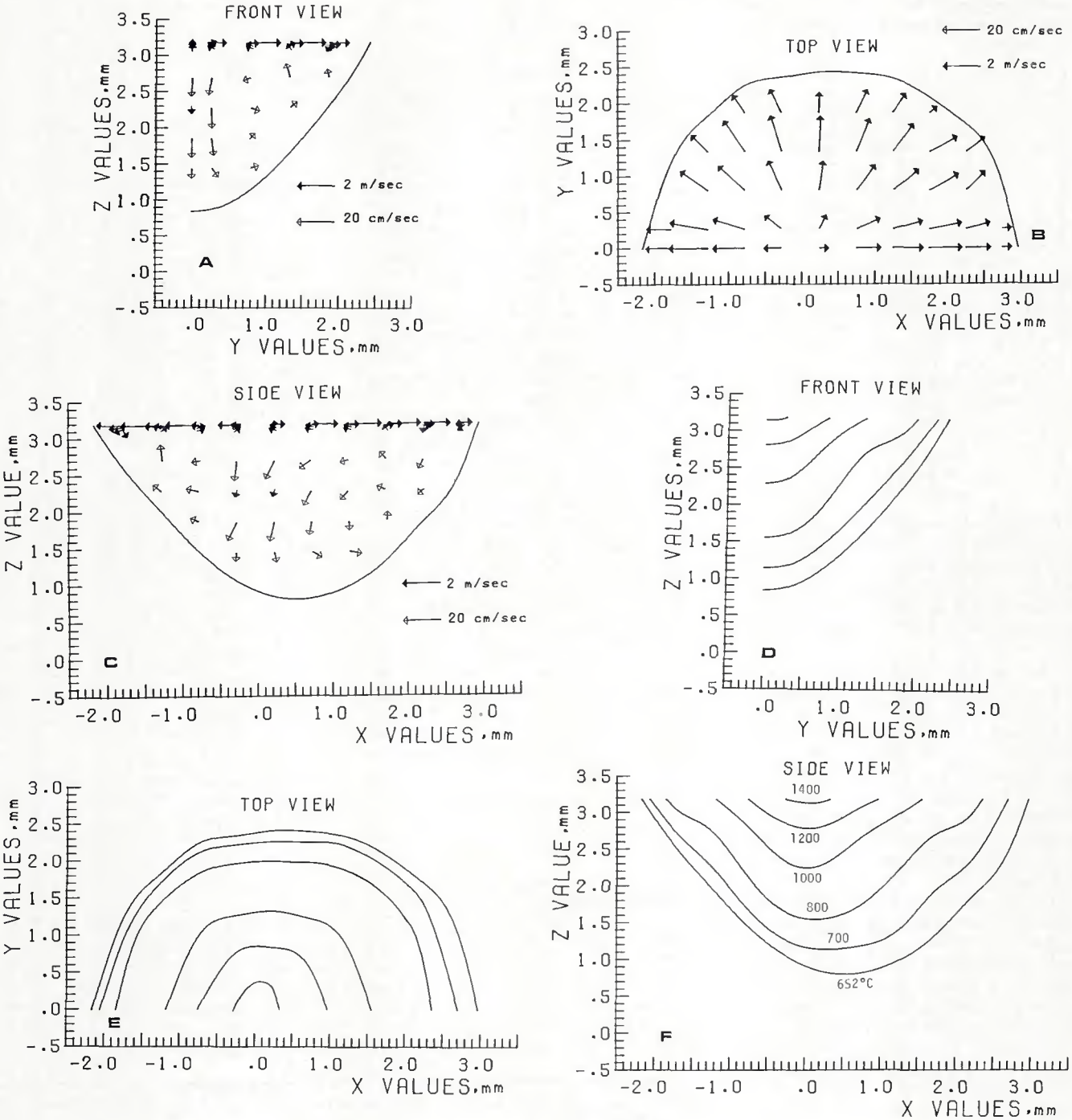

Fig. 3 — Velocity and temperature fields in the weld pool due to the combined action of the buoyancy force, the electromagnetic force and the surface tension gradient ($\partial\gamma/\partial T = -0.35$ g/s^2°C): (A–C) velocity fields; (D–F) temperature fields

Convection and Weld Penetration Due to Combined Driving Forces

Figure 3 shows the computed isotherms and convection patterns in the pool of the weld shown previously in Fig. 2. As can be seen in the front view of the convection pattern in Fig. 3A, there are two circulation loops in the weld pool: one near the free surface and the other in the bulk weld pool. The maximum velocity, which occurs at the free surface, is 2.3×10^3 mm/s (90.6 in./s). Figure 3B shows the top view of the convection pattern. As shown, flow at the free surface is radially outward, from the axis of the electrode (z-axis) to the pool boundary. Figure 3C shows the side view of the convection pattern. As shown, there are two circulation loops both ahead and behind the electrode, being consistent with the results shown previously in Fig. 3A. The corresponding isotherms are shown in Figs. 3D–3F.

Convection and Weld Penetration Due to Individual Driving Forces

In order to better understand the convection pattern shown previously in Fig. 3, which is the result of simultaneous action of all three driving forces, each of these driving forces was treated individually. Figure 4A shows the front view of the convection pattern due to the buoyancy force alone. For the lack of space, the top view, side view and isotherms are

not included here. The maximum velocity, which occurs at the free surface, is 9 mm/s (0.35 in./s).

Figure 4B shows the convection pattern due to the electromagnetic force alone. As shown, it is in the opposite direction of the buoyancy force driven flow shown in Fig. 4A. More importantly, the weld pool now penetrates the workpiece, indicating the strong influence of convection on weld penetration. The maximum velocity, which occurs along the axis of the electrode, is 1.8×10^2 mm/s (7.1 in./s).

Figure 4C shows the surface tension driven flow. The convection pattern is similar to that due to the buoyancy force alone, in that the pool is shallow, flow at the free surface is from center to boundary, and the maximum velocity occurs at the free surface. However, unlike the buoyancy force driven flow, the maximum velocity, 3.0×10^3 mm/s (118.1 in./s), is much higher, and the strength of convection below the free surface decays much more rapidly.

By comparing Fig. 4 with Fig. 3A, it becomes clear that the upper one of the double circulation loops in the latter is due to the surface tension gradient, while the lower one is due to the electromagnetic force.

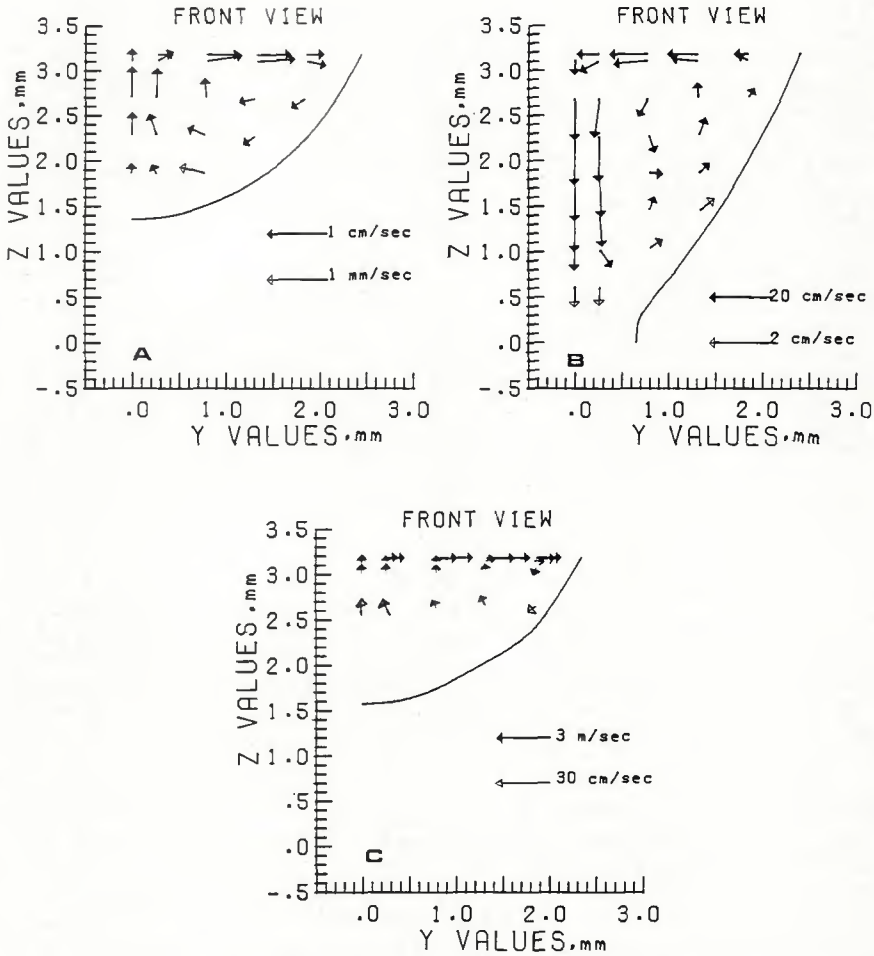

Fig. 4 — Velocity fields in the weld pool due to the individual action of (A) the buoyancy force; (B) the electromagnetic force; and (C) the surface tension gradient ($\partial\gamma/\partial T = -0.35$ g/s^2°C)

Convection and Weld Penetration Due to Modified Surface Tension Temperature Coefficient

In order to demonstrate the effect of the surface tension temperature coefficient $\partial\gamma/\partial T$ on weld pool convection and weld penetration, its value was changed from −0.35 to +0.35 g/s^2°C. As shown in Fig. 5, the convection pattern is reversed and full penetration is obtained. In fact, both the convection pattern and weld penetration resemble those shown previously in Fig. 4B for electromagnetically driven flow. The maximum velocity is 2.9×10^3 mm/s (114.2 in./s), and is at the free surface.

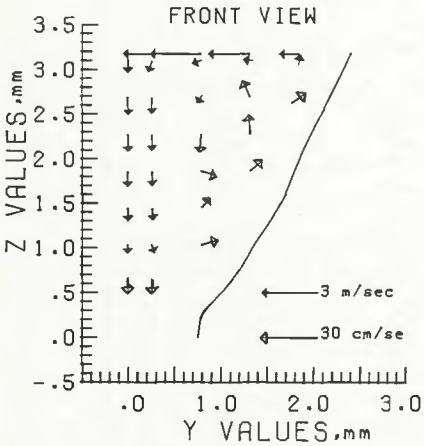

Fig. 5 — Velocity field in the weld pool due to the individual action of the surface tension gradient. $\partial\gamma/\partial T = 0.35$ g/s^2°C. Compare with Fig. 4

Figure 6 shows the results due to the combined driving forces. The input parameters are identical to those used previously for Fig. 3, except the value for $\partial\gamma/\partial T$ is changed to +0.035 g/s^2°C in this case. As shown, fluid flow on the free surface is now radially inwards and full penetration is produced.

Discussion

In this paper, a mathematical representation has been developed for heat transfer and convection in moving weld pools, considering three driving forces for convection: the buoyancy force, the electromagnetic force and the surface tension gradient. Attention is focused on how these three driving forces affect convection and weld penetration, both collectively and individually. Furthermore, based on the computed results, the effect of weld pool convection on macrosegregation and porosity in the weld metal is discussed.

The present work has been an important step forward, since heat flow and convection in stationary weld pools were first treated by Oreper, *et al.* (Ref. 7). Restrictions in the original work of Oreper, *et al.* (Ref. 7), such as stationary weld pools, known weld pool shapes, and semi-infinite workpieces, have now been released. As such, the present model is significantly more realistic and useful.

The principal findings in the present work may be described as follows:

Convection and Weld Penetration

1. This is the first time that detailed velocity and temperature distributions have been generated for moving weld pools during GTA welding. This information is being coupled with our ongoing studies on weld metal solidification and has so far been proved to be very useful.

2. In order to test the validity of the computer model, the arc efficiency and the spatial distributions of the electric current and heat flux used in the computations were based on experimentally

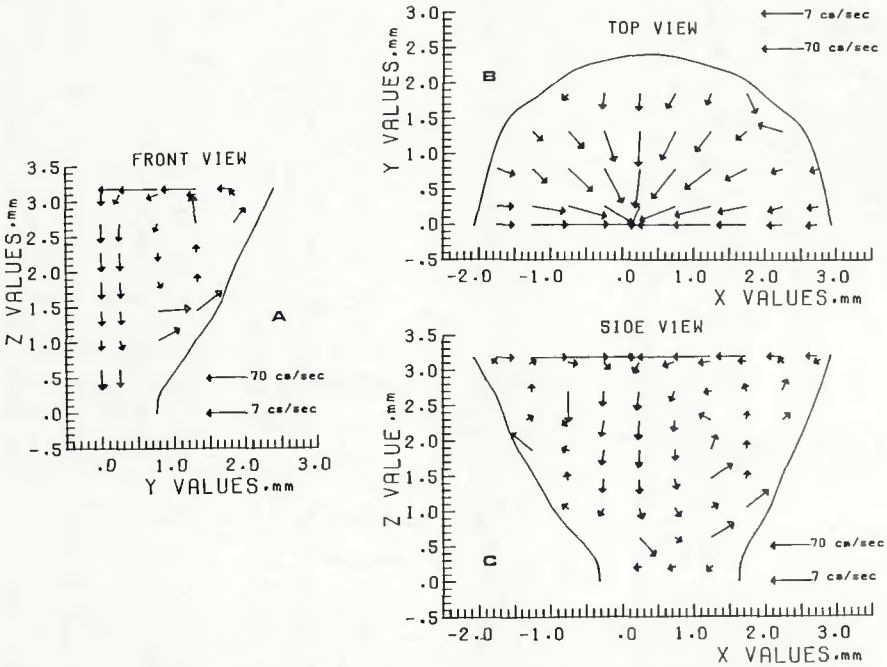

Fig. 6 — Velocity fields in the weld pool due to the combined action of the buoyancy force, the electromagnetic force and the surface tension gradient ($\partial\gamma/\partial T = 0.035\ g/s^2\,°C$): (A) front view; (B) top view; (C) side view

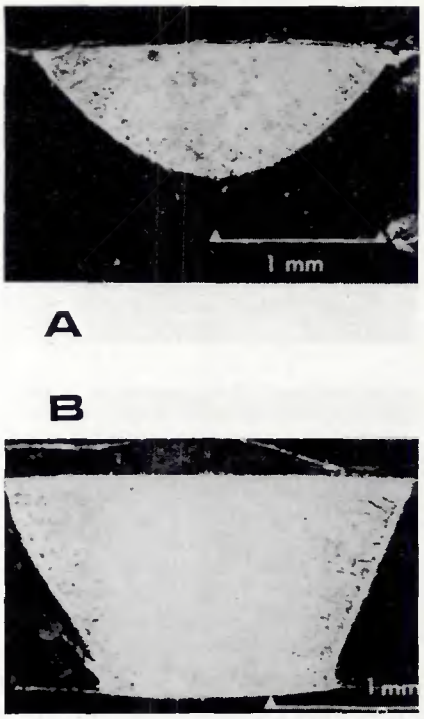

Fig. 7 — GTA welds of 304L stainless steel: (A) partial penetration weld made with pure Ar shielding gas; (B) full penetration weld made with Ar plus 700 ppm SO_2 shielding gas. From Heiple, et al. (Ref. 6)

measured results. The agreement between the computed and observed fusion boundaries is very good, thus verifying the validity of the model.

3. The convection patterns and weld penetration due to individual driving forces have been demonstrated separately to emphasize the distinct differences among themselves — Fig. 4. These individual convection patterns also help explain the one due to the combined driving forces (Fig. 3A), particularly with regard to the existence of the double circulation loops.

4. It is demonstrated clearly in this study that, under the same heat input and welding speed, weld penetration can be either full or partial, depending on the convection pattern in the weld pool. If the pattern is such that liquid metal flows downward from the top to bottom of the pool along the axis of the electrode, *e.g.*, Figs. 4B, 5 and 6, full penetration is more likely to occur. This is because this type of flow pattern favors the transfer of heat from the arc to the weld root, thus producing deeper penetration. When the surface flow pattern is radially outward, the downward flow of liquid metal from the top to the bottom of the pool is slowed down significantly and the resultant penetration is shallow. This can be seen by comparing Fig. 4B with Fig. 3A.

5. The effect of the surface tension temperature coefficient $\partial\gamma/\partial T$ on convection and weld penetration is clearly demonstrated. If $\partial\gamma/\partial T$, which is highly negative for both aluminum alloys and steels (Ref. 18), is made zero (Fig. 4B) or even positive (Fig. 5), weld penetration can switch from partial to full without having to increase the heat input. This is confirmed by the experimental results shown in Fig. 7, taken from the work of Heiple, *et al.* (Ref. 6). As shown, with a very small addition of $SO_2(g)$ in the argon shielding gas, GTA welds in 304L stainless steel changed from partial to full penetration. Both sulfur and oxygen, which are produced by the decomposition of $SO_2(g)$ in the arc, are surface active agents for liquid iron and tend to reduce or even reverse its surface tension vs. temperature relationship (Ref. 2). Although similar surface active agents are not known in aluminum alloys, the effect of $\partial\gamma/\partial T$ demonstrated in this study is equally applicable to all materials.

It should be pointed out that in the previous experimental work of Heiple, *et al.* (Ref. 2), shallower penetration was observed in weld pools exhibiting a radially outward surface flow pattern, while deeper penetration was observed in weld pools exhibiting a radially inward surface flow pattern. This is consistent with the computed results shown in Figs. 3 and 6.

6. The maximum velocity in the case of surface tension driven or surface tension dominated flow is on the order of 10^3 mm/s (39.4 in./s). Surface velocities of this order of magnitude have been reported previously by Heiple, *et al.* (Ref. 2). The maximum velocities due to the electromagnetic and the buoyancy forces are essentially on the order of 10^2 and 10 mm/s, respectively. It should be pointed out that high velocities are restricted to rather small regions in the case of surface tension driven flow. Therefore, the characteristic length in the Reynolds number should be much smaller than the depth or width of the weld pool itself, thus still resulting in small enough Reynolds numbers to indicate laminar flow in the weld pool. This has been discussed in previous studies of Oreper, *et al.* (Ref. 7), and Kou, *et al.* (Ref. 8). However, it is recognized that turbulence can exist in pools of larger size when much higher welding currents are used.

Macrosegregation

1. In continuous welds made with the addition of filler metals, macrosegregation can occur, especially in the plane transverse to the weld, if mixing in the weld pool is insufficient. In arc welding, the electromagnetic force tends to promote mixing in the bulk weld pool. As can be seen in Fig. 4B, the filler metal added to the center of the top surface can be quickly transferred to the bottom of the weld pool, then pushed up to the top surface along the fusion boundary, and finally driven back to the center. This mixing action, based on the computed velocity distribution in the bulk weld pool, takes approximately 0.1 ~ 0.2 s. Since in this example the computed length of the weld pool is about 5 mm

(0.2 in.) and the welding speed is about 5 mm/s (0.2 in./s), the weld metal remains in the liquid state for about 1 s before it solidifies. From the estimations made above, it can be expected that the weld metal will be well mixed before it solidifies and that there will be no significant macrosegregation in the bulk weld metal. Similar conclusions can be drawn from Fig. 3A, which shows a double-circulation-loop convection pattern due to the combined action of all three driving forces. It can be expected that uniform surface composition can be achieved instantaneously by the upper circulation loop induced by the surface tension gradient, in view of the very high velocities present. However, this circulation loop should not prevent the filler metal from being mixed in the bulk weld pool. This is because the filler metal droplets, with the momentum they gain from the arc plasma and the gravity force, can easily penetrate the free surface and join the lower circulation loop in the bulk weld pool induced by the electromagnetic force. In fact, this momentum can actually enhance the mixing action in the weld pool and further insure uniform composition in the bulk weld metal.

The above discussion is consistent with the macrosegregation study of Houldcroft (Ref. 21), which indicates uniform composition in the bulk fusion zone of aluminum welds made with dissimilar filler metals, as shown in Fig. 8A.

In the joining of thin sheets of dissimilar metals, the weld pools tend to have a rather low depth/width ratio, and the welding current is kept low to avoid burning through. This sometimes causes weld macrosegregation, and externally applied electromagnetic stirring has been adopted to insure uniform composition (Ref. 22).

2. Although in most arc welds the composition of the bulk fusion zone is quite uniform, there exists a thin layer of liquid metal near the pool boundary in which very little mixing occurs, as can be seen, for instance, from Figs. 3A and 3C. This results from the physical requirement that the velocity of the liquid metal relative to the pool boundary should be zero there. This thin layer of unmixed liquid metal is responsible for the formation of the unmixed zone reported by Savage, *et al.* (Refs. 23, 24), as shown in Fig. 8B. The composition in this zone differs significantly from that of the bulk fusion zone. The effect of this unmixed zone on the properties of the weld is described in detail in the text by Kou (Ref. 25).

3. In laser beam welding with the surface melting mode, weld pool convection is dominated by the surface tension gradient at the weld pool surface. Unlike electromagnetic force induced flow, surface tension induced flow is most pronounced only near the free surface, as shown in Fig. 4C. As a result, mixing in the bulk weld pool can be poor. This is consistent with the work of Seretsky, *et al.* (Ref. 26), which indicates poor mixing in laser beam welds of dissimilar metals, as shown in Fig. 8C. It should be pointed out that the poor mixing action in laser beam weld pools can be made worse by the high welding speeds used in laser beam welding.

If surface active agents are present in the weld pool, surface tension induced convection can penetrate deep into the weld pool, as shown in Fig. 5. As a result, much better mixing in the weld pool, and hence better homogeneity in the bulk weld metal, can be expected.

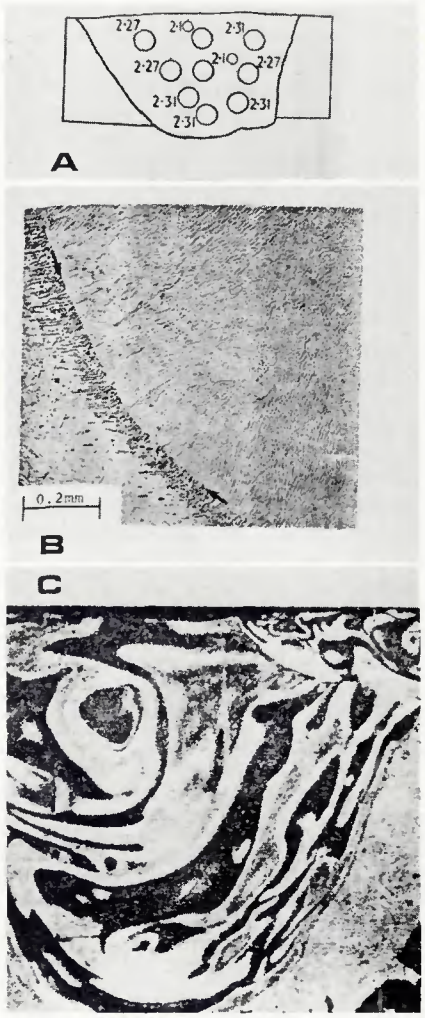

Fig. 8 — Macrosegregation in welds: (A) essentially uniform composition in the bulk fusion zone of pure Al arc welded with Al-5% Cu filler, from Houldcroft (Ref. 21); (B) evidence of the unmixed zone along the fusion boundary of 304 stainless steel arc welded with 310 filler, from Lippold and Savage (Ref. 24); (C) lack of mixing in a Ti-Ni dissimilar weld produced by laser, from Seretsky and Ryba (Ref. 26), magnification 70X

Porosity

The computed convection patterns in this work can also be applied to the problem of gas porosity in the weld metal. It is often considered true that weld pool convection always helps reduce weld porosity. This, in fact, is not true, as can be demonstrated with the help of the schematic sketch shown in Fig. 9. The gas forming constituents, such as H in aluminum or C and O in steels, have a much lower solubility in the solid weld metal than in the liquid metal. Consequently, these constituents are rejected into the liquid metal ahead of the solidification front and form gas bubbles. In Fig. 9A, the convection pattern is such that it produces a downward sweeping action on the gas bubbles formed near the fusion boundary, as in the case of buoyancy force induced flow or surface tension induced flow in the absence of surface active agents. Many gas bubbles can be caught up by the solidification front and become gas pores in the solidified weld metal. As such, this type of convection pattern does not help reduce weld porosity; in fact, it might even be detrimental. In Fig. 9B, on the other hand, the convection pattern is such that it produces an upward sweeping action on the gas bubbles, as in the case of electromagnetically induced flow or surface tension induced flow in the presence of surface active agents. Many gas bubbles can reach the free surface and escape from the weld pool before being caught up by the solidification front, thus resulting in a porosity level lower than that in the previous case. Further experimental work, however, is needed to verify this postulation.

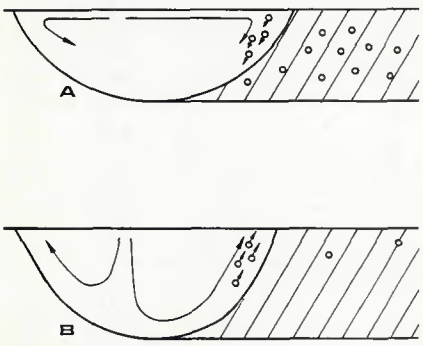

Fig. 9 — Effect of weld pool convection on weld porosity: (A) convection pattern favoring trapping of gas bubbles; (B) convection pattern favoring removal of gas bubbles

Conclusion

The model presented in this paper describes quantitatively, for the first time, heat flow and convection in moving weld pools. It incorporates three distinct driving forces for flow: the buoyancy force, the electromagnetic force and the sur-

face tension gradient. It is applicable to workpieces of finite thickness, thus allowing both partial- and full-penetration welds to be considered. The "a priori" specification of the well pool shape is not necessary, as the model is capable of computing it.

Very good agreement was obtained between computed and experimentally observed fusion boundaries, thus verifying the validity of the model. The arc efficiency and the spatial distributions of the electric current and heat flux used in the computations were based on experimentally measured results, in order to make sure that the verification was appropriate.

The convection patterns and weld penetrations due to individual driving forces were demonstrated separately, in order to show the distinct differences among themselves and to help explain those due to the combined driving forces, especially the double circulation loops.

The model is consistent with the recent work of Heiple, *et al.* (Ref. 6), which shows that, under the same heat input and welding speed, welds can be made to change from partial to full penetration by modifying the surface tension temperature coefficient $\partial\gamma/\partial T$ of the weld pool through the application of surface active agents. It also agrees with the earlier work of Heiple, *et al.* (Ref. 2), which shows shallower penetration in weld pools exhibiting a radially outward surface flow pattern, but deeper penetration in weld pools exhibiting a radially inward surface flow pattern. Maximum surface velocities on the order of 10^3 mm/s (39.4 in./s), reported in the same work of Heiple, *et al.* (Ref. 2), are also confirmed.

According to the computed velocity distributions in arc weld pools, the time required for mixing liquid metal in the bulk weld pool is much shorter than the time the weld metal remains in the liquid state before it solidifies, due to electromagnetically induced convection. This agrees with the experimental work of Houldcroft (Ref. 21), which shows little macrosegregation in the bulk fusion zone of arc welds. The same computed results, however, reveal the lack of mixing in a thin liquid metal layer near the fusion boundary, confirming the existence of the unmixed zone reported by Savage, *et al.* (Refs. 23, 24).

According to the computed results for surface tension driven convection, mixing in the bulk weld pools can be poor in laser beam welding with the surface melting mode. This is consistent with the work of Seretsky, *et al.* (Ref. 26), which shows poor mixing in laser beam welds of dissimilar metals.

Finally, based on the computed convection patterns, it is postulated that electromagnetically induced convection or surface tension induced convection under the influence of surface active agents tends to sweep gas bubbles toward the free surface and help them escape from the weld pool before being caught up by the solidification front, while buoyancy induced convection or surface tension induced convection in the absence of surface active agents does the opposite. Further work is needed to verify this postulation and the expected difference in gas porosity.

Acknowledgments

The authors gratefully acknowledge support for this study from the National Science Foundation, under NSF Grant No. DMR 8419274. The initial support for this work was from the Graduate School, University of Wisconsin—Madison.

References

1. Heiple, C. R., and Roper, J. R. 1981. Effect of selenium on GTAW fusion zone geometry. *Welding Journal* 60(8): 143-s to 145-s.

2. Heiple, C. R., and Roper, J. R. 1982. Mechanism for minor element effect on GTA fusion zone geometry. *Welding Journal* 61(4): 97-s to 102-s.

3. Heiple, C. R., and Roper, J. R. 1982. Effects of minor elements on GTAW fusion zone shape. *Trends in Welding Research in the United States*, S. A. David, ed. 489–520. American Society for Metals, Metals Park, Ohio.

4. Heiple, C. R., Roper, J. R., Stagner, R. T., and Aden, R. J. 1983. Surface active element effects on the shape of GTA, laser and electron beam welds. *Welding Journal* 62(3): 72-s to 77-s.

5. Heiple, C. R., Burgardt, P., and Roper, J. R. 1984. The effect of trace elements on GTA weld penetration. *Modeling of Casting and Welding Processes II*, J. A. Dantzig and J. T. Berry, eds. 193–205. TMS-AIME, Warrendale, Pa.

6. Heiple, C. R., and Burgardt, P. 1985. Effects of SO_2 shielding gas additions on GTA weld shape. *Welding Journal* 64(6): 159-s to 162-s.

7. Oreper, G. M., Eagar, T. W., and Szekley, J. 1983. Convection in arc weld pools. *Welding Journal* 62(11): 307-s to 312-s.

8. Kou, S., and Sun, D. K. 1985. Fluid flow and weld penetration in stationary arc welds. Metallurgical Transactions A, 16A(2): 203.

9. Oreper, G. M., and Szekely, J. 1984. Heat- and fluid-flow phenomena in weld pools. *Journal of Fluid Mechanics* 147(10): 53.

10. Chan, C., Mazumder, J., and Chen, M. M. 1984. A two-dimensional transient model for convection in laser melted pools. Metallurgical Transactions A, 15A(12): 2175.

11. Kou, S., Le, Y., and Lu, M. 1985. Ongoing research at University of Wisconsin, Madison, Wis.

12. Kou, S., and Lu, M. Efficiency of welding heat sources. To be published.

13. Kou, S., and Lu, M. Spatial distributions of heat flux and electric current in gas-tungsten arcs. To be published.

14. Lawson, W. H. S., and Kerr, H. W. 1976. Fluid motion in GTA weld pools: part II—weld pool shapes. *Welding Research International.* Vol. 6, Paper No. 6, p. 1.

15. Lin, M. L., and Eagar, T. W. 1985. Influence of arc pressure on weld pool geometry. *Welding Journal* 64(6): 163-s to 169-s.

16. Kou, S., and Le, Y. 1983. Three-dimensional heat flow and solidification during the autogenous GTA welding of aluminum plates. Metallurgical Transactions A, 14A(11): 2245.

17. Kou, S., and Wang, Y. H. 1985. Simulation of weld pool convection in arc welding. To be published.

18. Allen, B. C. 1972. The surface tension of liquid metals. *Liquid Metals—Chemistry and Physics*, S. Z. Beer, ed. 161-212. M. Dekker, Inc., New York, N.Y.

19. *Aluminum Standards and Data*, fifth edition. 1976. The Aluminum Association, New York, N.Y., pp. 38 and 40.

20. *Aluminum*, K. R. Van Horn, ed. 1967. ASM, Vol. 1, Chapter 1, pp. 1–30.

21. Houldcroft, R. T. 1954. Dilution and uniformity in aluminum alloy weld beads. *British Welding Journal* 1: 468.

22. Matsuda, F., Ushio, M., Nakagawa, H., and Nakata, K. 1980. Effects of electromagnetic stirring on the weld solidification structure of aluminum alloys. *Proceedings of the Conference on Arc Physics and Weld Pool Behavior*, Vol. 1, p. 337, The Welding Institute, Cambridge, U.K.

23. Savage, W. F., Baeslack III, W. A., and Lippold, J. C. 1979. Unmixed zone formation in austenitic stainless steel weldments. *Welding Journal* 58(6): 168-s to 176-s.

24. Lippold, J. C., and Savage, W. F. 1980. Solidification of austenitic stainless steel weldments: part II. *Welding Journal* 59(2): 48-s to 58-s.

25. Kou, S. Welding Metallurgy. To be published by John Wiley and Sons, Inc., New York, N.Y.

26. Seretsky, J., and Ryba, E. R. 1976. Laser welding of dissimilar metals. *Welding Journal* 55(7): 208-s to 211-s.